Characterization of optical and structural properties of GaAsN layers grown by Molecular Beam Epitaxy

A. Pulzara-Mora[a], E. Cruz-Hernández, J. Rojas-Ramirez, R. Contreras-Guerrero, M. Meléndez-Lira, C. Falcony-Guajardo and M. López-López
Physics Department, Centro de Investigación y Estudios Avanzados del IPN
Apartado Postal 14-740, México D.F, México 07000.

M. A. Aguilar-Frutis
Centro de Investigación en Ciencia Aplicada y Tecnología Avanzada, IPN, Legaria, Mexico

M. A. Vidal
Instituto de Investigación en Comunicación Optica, UASLP, San Luis Potosí, México

[a] *Departamento de Física y Química, Universidad Nacional de Colombia, Sede Manizales*
(Recibido: 13 de julio de 2005; Aceptado: 31 de agosto de 2005)

GaAsN layers were grown on GaAs(100) substrates by MBE employing a radio frequency (RF) plasma nitrogen source, and solid sources for Ga and As. The growth temperature was varied from 420 to 600 °C, and the GaAsN growth mode was *in-situ* monitored by reflection high-energy electron diffraction (RHEED). The optical properties of the layers were studied by photoreflectance spectroscopy (PR), phase modulated ellipsometry (PME), and photoluminescence. For the growth temperature of 420 °C the films grew in a three-dimensional (3D) mode as indicated by the appearance of transmission spots in the RHEED patterns. In contrast, GaAsN layers grown at higher temperatures presented a two-dimensional (2D) growth mode. These GaAsN layers are pseudomorphic according to high resolution x-ray diffraction (HRXRD). The PR spectra of all samples exhibited Franz-Keldish oscillations (FKO) above of the GaAs band-gap energy. From these oscillations we obtained the built-in internal electric field intensity (F_{int}) at the GaAsN/GaAs interface. In the low energy region of the PR spectra we observed the transitions associated to the fundamental band-gap of the $GaAs_{1-x}N_x$ layers. The variation of the GaAsN fundamental band-gap obtained by PR as a function of the N content was explained according the band anticrossing model (BAC). On the other hand, the E_1 and $E_1+\Delta E_1$ critical points were obtained from the analysis of spectra of the imaginary part of the dielectric function obtained by PME. We observed a shift of these critical points to higher energies with the increase of N content, which was explained by a combination of strain and alloying effects.

Keywords: III-V-N semiconductors; MBE; Optical properties; Structural characteristics

1. Introduction

Currently there is considerable interest in III-V-N dilute nitride thin film alloys, such as GaAsN, both because of their fundamental physical properties and potential device applications [1]. The substitution of a few percent of As atoms in GaAs by N atoms leads to a strong reduction of the band gap energy, for example; for 1% N added to GaAs the band gap energy is reduced by ~200 meV [2]. This characteristic makes GaAsN alloys very attractive for applications in 1.3/1.55 μm semiconductor lasers, and for extending the wavelength range of GaAs-based solar cells further into the infra-red. There has been substantial progress in the synthesis of GaAsN alloys by molecular beam epitaxy (MBE). However, in order to obtain reproducible high quality dilute nitride thin films additional studies on the alloys growth and their properties are required.

It is well known that in the heteroepitaxial growth of materials with a small lattice mismatch the epilayer can be grown pseudomorphically, that is with the same in-plane lattice constant of the substrate, up to certain critical thickness which depends on the lattice mismatch value and on elastic properties of the materials. In order to obtain pseudomorphic layers an appropriate growth mode is required to avoid lattice mismatch strain relaxation by the introduction of crystal defects. This is particular important for device applications since crystal defects strongly deteriorate the performance of devices. In this work we have studied the effects of growth temperature on the growth mode of GaAsN layers on GaAs(100) substrates. We evaluated the optical properties of GaAsN thin films grown at different temperatures.

2. Experimental

The $GaAs_{1-x}N_x$ layers in this work were grown on (100) GaAs substrates employing a Riber C21 MBE system equipped with solid sources for III-V materials, and a standard reflection high-energy electron diffraction (RHEED) system. Nitrogen atoms were produced by a radio frequency (RF) plasma source. Ultrahigh purity

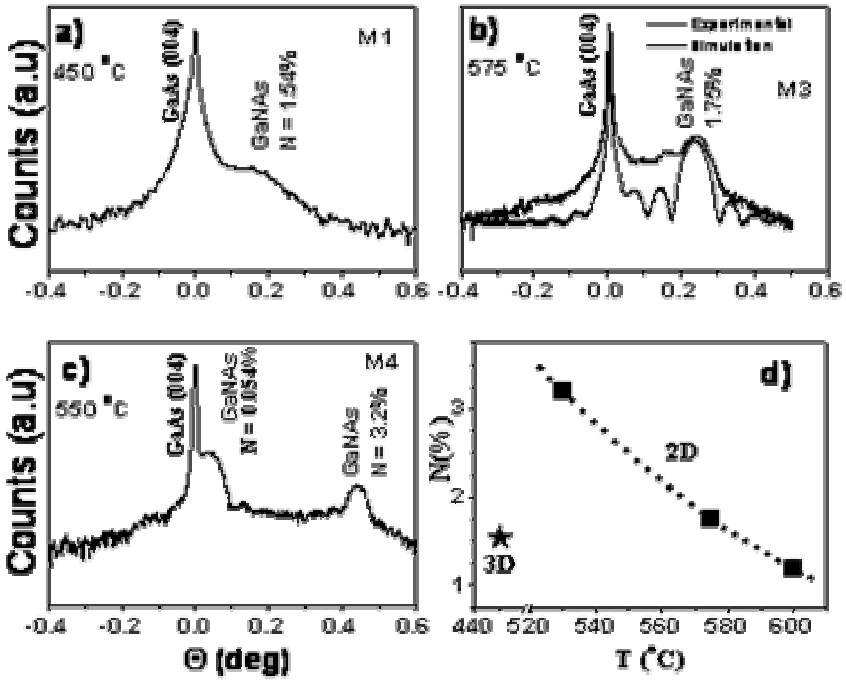

Figure 1. HRXRD rocking curves of GaNAs samples grown at different temperatures. (d) Shows the nitrogen composition as a function of growth temperature.

nitrogen was introduced into the plasma source using a mass flux controller and a leak valve. First, in the MBE chamber the substrates were heated up to 580 °C to remove the surface oxides under an As_4 flux. Then, in order to smooth out surface imperfections, a GaAs buffer layer was grown at 580 °C. At end of the buffer layer growth the surface exhibited a sharp (2x4) RHEED pattern. After the buffer layer growth, the growth temperature was fixed to the desired value, and the N plasma was ignited to grow the GaAsN alloy. GaAsN layers were prepared at different growth temperatures with the same thickness (~100 nm), using a growth rate of 1μm/hr. The plasma excitation power and the N_2 flow were held constant at 100 W and 0.1 sccm, respectively. The GaAsN growth mode was *in-situ* monitored by RHEED. High resolution x-ray diffraction (HRXRD) measurements were performed using a Phillips diffractometer with a copper anode. Photoluminescence spectroscopy (PL) was realized at 10 K employing an Ar laser of wavelength $\lambda = 488$ nm. The fundamental band gap energy of GaAsN layers was studied by photoreflectance spectroscopy (PR) employing a standard experimental setup, with modulation light provided by a He-Ne laser of wavelength $\lambda = 632.8$ nm. The chopped laser light was irradiated onto the sample by a spot radius of ~ 1 mm. A 200 W tungsten lamp was dispersed by a 20-cm monochromator and used as a probe light. The reflected probe light from the sample was detected by a Si detector, and the signal from the detector was fed to a lock-in amplifier. Higher energy transitions were studied employing a spectroscopic phase modulated ellipsometer.

3. Results and discussion

The structural properties and the Nitrogen content of GaAsN layers grown at different temperatures were analyzed by HRXRD. Figures 1(a)-(c) show (400) rocking curves of GaAsN layers grown at 450 (M1), 575 (M3) and 550°C (M4), respectively. A graded structure was employed for the sample M4, in this sample a 100 nm thick GaAsN layer with a low N content was first grown to smooth the growth transition from GaAs to GaAsN. From the HRXRD rocking curves we obtained N compositions of 1.54%, 1.75%, and 0.05% / 3.2%, for samples M1, M3 and M4, respectively. The HRXRD curve corresponding to sample M1 shows a broad peak for the GaAsN layer indicating poor crystal quality, which is presumably caused by the 3D growth observed in this sample, as will be discussed below. For sample M3 Pendellosung fringes are observed in the rocking curve, as indicated by the dynamical theory simulation curve (thin line in Fig. 2(b)), this result shows a high crystalline quality layer with a smooth and abrupt GaAsN/GaAs interface. The rocking curve for sample M4 clearly shows the two peaks corresponding to the two GaAsN layers with different N concentration. Pendellösung fringes can also be observed in this sample with a high N composition layer on top of a GaAsN layer with a low N content. Figure 1(d) shows the nitrogen composition as a function of growth temperature obtained from HRXRD. In this figure we have included sample M2 (N%=1.18) grown at 600 °C.

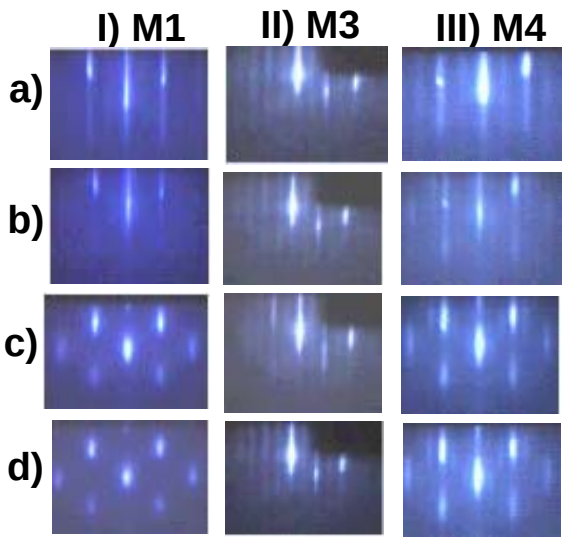

Figure 2. RHEED patterns during the GaAsN alloys growth at: I) 420 ºC II) 575 ºC,and III) 550 ºC. a) GaAs buffer layer surface, b) just after the start of GaAsN growth, c) 7 ML of growth, and d) at the end of growth (100 nm).

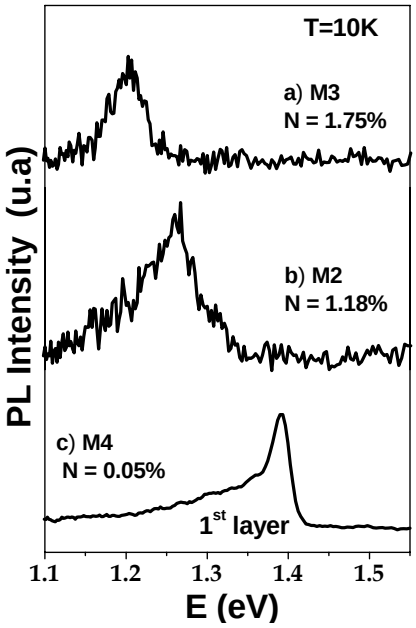

Figure 3. Photoluminscence spectra at 10 K of GaAsN layers grown on GaAs substrates.

In the Fig. 2, we present a sequence of RHEED patterns, taken along the substrate [011] azimuth, during the growth of GaAsN layers at: I) 450 ºC (sample M1), II) 575 ºC (sample M3), and III) 550 ºC (sample M4). In this figure the RHEED patterns correspond to: a) GaAs buffer layer surface, b) just after start of GaAsN growth, c) 7 ML of growth, and d) at the end of growth (100 nm). The initial GaAs surface exhibited a c(4x4) surface reconstruction below 560 °C, above this temperature a (2x4) surface reconstruction was observed. According to HRXRD measurements the samples are pseudomorphic, except for sample M1. For this sample when the GaAsN growth commenced transmission spots appeared in the RHEED patterns (Fig. 2. I b-c), indicating a roughening of the surface probably caused by the formation of GaAsN clusters. According to these results, GaAsN grows in a 3D mode at low temperatures, which could be caused by the low surface mobility of adatoms. On the other hand, streak RHEED pattern for the sample M3 were conserved during all the GaAsN growth (Fig. 2 II b-d). This behavior indicates us that at high growth temperatures a two dimensional (2D) growth mode is maintained. Moreover, the 2x4 reconstruction was observed during all the GaAsN growth, suggesting that for this sample N atoms have little effect on the surface atomic arrangement. For the sample M4 grown at 550 ºC, streaky patterns where also observed during GaAsN growth (Fig. 1. III. b-d). For this sample a (3x3) surface reconstruction was observed during the GaAsN growth, indicating that the high N content produces considerable changes in the surface atomic arrangement. From the HRXRD and RHEED results we conclude that for the samples grown in a 2D mode the nitrogen composition decreases when the substrate temperature is increased as observed in Fig. 1 (d). This result can be explained considering an enhanced evaporation of N atoms on the sample surface at high growth temperatures.

Now we present the results of the optical characterization of the samples. Fig. 3 shows PL spectra for samples M2, M3 and M4, grown in 2D mode. For samples grown in 3D mode no PL signal was detected showing a high density of non-radiative recombination centers. In Fig. 3 we note that the emission peak shifts towards lower energies when the nitrogen content in the samples increased indicating a decrease in the band gap energy. In order to study the fundamental band gap variation as a function of N content in GaAsN layers we performed PR measurements. Fig. 4 shows PR spectra of samples M1-M4 obtained at room temperature. The insets in the Fig. 4 show an enlargement of the spectra in the GaAsN fundamental band gap region. In the spectra we observe the band gap transition from the GaAs buffer layer at ~1.42 eV. Above this energy the PR signal exhibits oscillations identified as Franz-Keldish oscillations (FKO), which are produced by intense built-in electric fields [3]. In the low energy region of the spectra we observe the transition associated to fundamental band gap (indicated by arrows in Fig. 4) of the $GaAs_{1-x}N_x$ layers.

Note that the PR spectrum of the graded sample (M4) has two transitions below the GaAs band gap associated to the two GaAsN layers: the first transition is at 1.36 eV corresponding to the layer with N = 0.05%, and the second transition is at 1.1 eV corresponding to the layer with N =3.2%. Since the PR signal intensity depends on the built-in electric field, the larger amplitude of the GaAsN transition in sample M1 could be the result of a high intensity internal electric field in this sample. A signature of a high intensity electric field in sample M1 is the presence of clear FKO above the GaAsN band gap

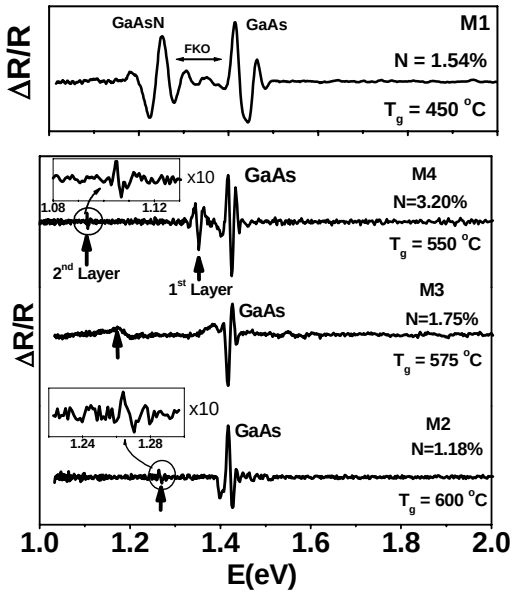

Figure 4. Photoreflectance spectra at room temperature of GaAsN layers. The insets show an enlargement of the spectra in the GaAsN fundamental band-gap region.

transition, as indicated in Fig. 4. From an analysis of the FKO is possible to determine the strength of the built-in internal electric field present in the samples. The FKO amplitude extrema occur at energies (E_j) given by [4]:

$$E_j = \hbar\Omega F_j + E_g \tag{1}$$

where

$$F_j = \left[\frac{3}{2}\pi\left(j-\frac{1}{2}\right)\right]^{2/3} \qquad j=1,2 \tag{2}$$

$\hbar\Omega$ is a characteristic electro-optic energy given by :

$$\hbar\Omega = \left(\frac{e^2 F_{int}{}^2 \hbar^2}{8\mu}\right)^{1/3} \tag{3}$$

F_{int} is the built-in electric field strength, and μ is the interband reduced mass involved in the transition.

From Eq. (1) we observe that a plot of E_j vs F_j corresponds to the equation of a straight line, taking the line slop we can obtain the built-in electric field F_{int} by Eq. (3), and from the ordinate to origin we obtain the material band gap energy E_g.

This analysis is shown in the inset of Fig. 3 for the sample grown at 450 °C, for FKO associated to GaAs and GaAsN. The built-in internal electric field intensity (F_{int}) calculated from the analysis of FKO associated to GaAs and to GaAsN is shown in Fig. 5 as a function of nitrogen content. The F_{int} values obtained for samples grown in 2D and 3D modes are plotted by squares (■) and stars (★) symbols, respectively.

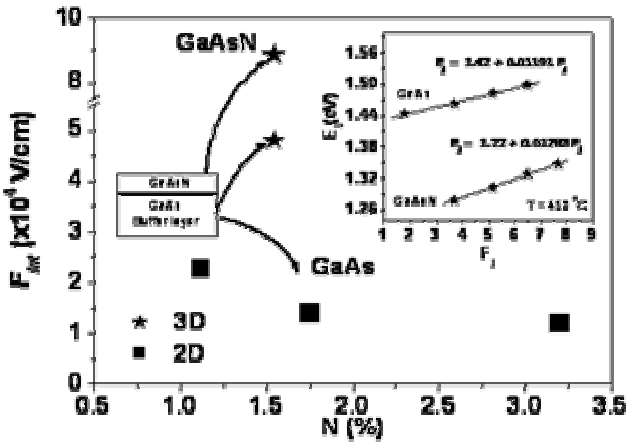

Figure 5. Built-in internal electric field intensity F_{int} in GaAs and in GaAsN for samples grown in two-dimensional (■) and three-dimensional (★) mode. The inset shows the linear fittings of the energy extremes in the FKO oscillations for the sample grown at 450 °C.

We note that the electric field intensity for the 3D-grown sample (M1) is larger than for 2D-grown samples. Crystal defects in the relaxed M1 sample could be the cause of the more intense electric fields in this sample. On the other hand in 2D-grown samples the electric field is around $2\text{x}10^4$ V/cm, which is the typical value found in MBE grown GaAs layers [5].

We calculated the GaAsN alloys fundamental band gap ($E_g(GaAsN)$) by the band anti-crossing model (BAC) [6], employing the nitrogen concentrations extracted by HRXRD. We took into consideration the following correction to $E_g(GaAsN)$ related to strain for the samples with 2D growth mode:

$$Eg(GaAsN) = Eg_{BAC} + \delta E_H - \delta E_S \tag{4}$$

where Eg_{BAC} is the bandgap calculated from the BAC model and δE_H and δE_S are the hydrostatic pressure shift and uniaxial stress shift defined by [7]:

$$\delta E_H = 2a\frac{C_{11}-C_{12}}{C_{11}}\varepsilon \tag{5}$$

$$\delta E_S = b\frac{C_{11}+2C_{12}}{C_{11}}\varepsilon \tag{6}$$

where a and b are the interband hydrostatic pressure and uniaxial deformation potentials, respectively. C_{ij} are elastic-stiffness constants, and ε is the biaxial strain.

The values for the GaAsN band gap obtained from Eq (4) are 1.26, 1.17, and 1.1 eV for samples M2, M3, and M4, respectively. As shown in Fig. 2 these values are in good agreement with the GaAsN transitions observed in the PR spectra, which were obtained by fitting the experimental data to a third derivative functional form [4].

Fig. 6 (a) shows the complex dielectric function $<\varepsilon_2>$ of samples M1- M4, and of a control GaAs sample without nitrogen content. The solid lines represent the experimental

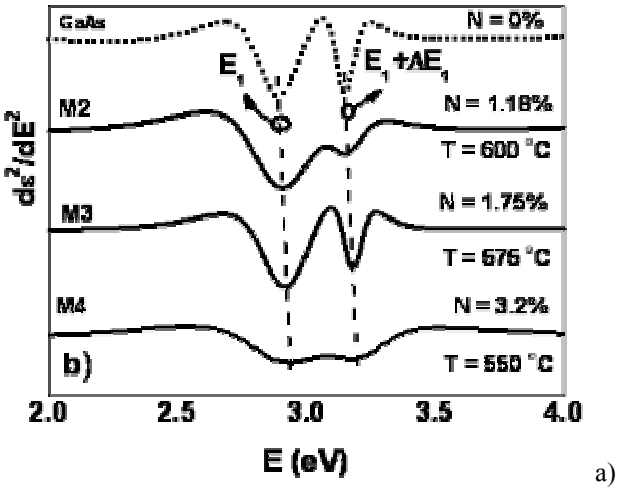

a)

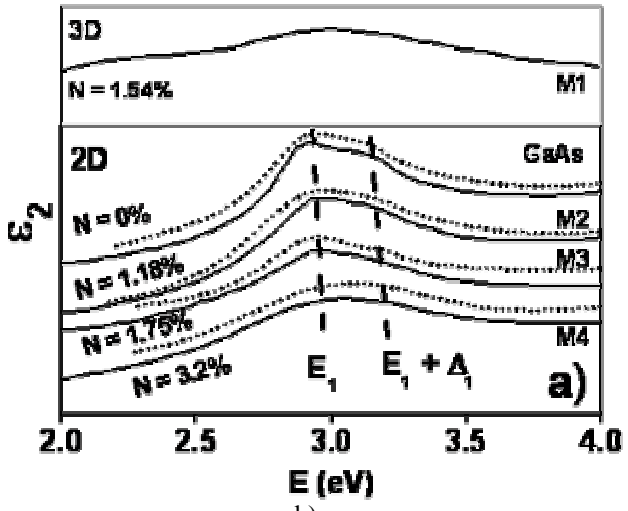

b)

Figure 6. a) Experimental data (solid lines) of the imaginary part $<\varepsilon_2>$ of tl dielectric function for GaAsN samples. The dotted lines are the fittin obtained by using the Adashi's model. The spectrum of a control GaA sample (cero N content) is also included in the figure. b) Second derivative the imaginary part $<\varepsilon_2>$ of the dielectric function.

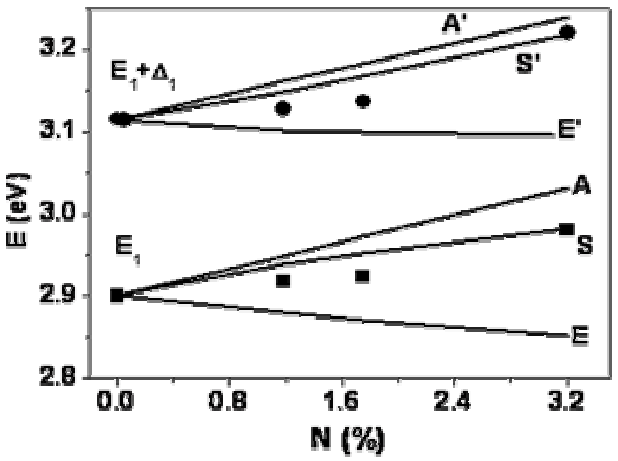

Figure 7. E_1 and $E_1+\Delta_1$ critical point energies as a function of N content. The lines E and E' are theoretical calculation of the stress effects in the GaAsN layers. The lines A and A' are the alloying effect by Vegard's law, and lines S and S' show the combined effect of stress and alloying.

data, and the dotted lines are the best fit calculation by using the Adashi Model [8]. For sample M1 the spectrum has a low intensity and the optical transitions are very wide. The poor crystal quality in this sample makes difficult the analysis of the critical points. The main features in the spectra are the optical transitions termed E_1 and $E_1+\Delta_1$. By taking the second derivative of the fitted dielectric function spectra we obtained E_1 and $E_1+\Delta_1$, as indicating in the Fig. 6 (b). In this figure, we observed that the E_1 and $E_1+\Delta_1$ transitions in the GaAsN alloys shift to high energies with increasing nitrogen content in the samples. This shift is originated by the combined effects of strain and alloying in the films [9]. The strain produces a red shift that can be estimated for E_1 by:

$$\delta E_1 = \Delta_1 / 2 + \delta E_H - \sqrt{(\Delta_1 / 2)^2 + (\delta E_S \pm \Delta E_{ex})^2} \qquad (7)$$

where δE_H and δE_S are defined by Eqs. (5) and (6), and ΔE_{ex} is the electron-hole spin-exchange term. The results of the calculated strain induced red shifts are shown by lines E and E' in Fig. 7. On the other hand, the shifts produced by alloying were calculated by using the Vegard′s law between GaAs (N=0%) and GaN (N=100%), for GaN we took the E_1 and Δ_1 values for the cubic structure [10]; the results are indicated by the lines A and A' in Fig 7. In this figure the lines S and S' shows the combined effects of stress and alloying obtained by adding both effects. The results of Fig. 6(b) are plotted by square symbols (E_1) and dots ($E_1+\Delta_1$) in Fig. 7. We note a reasonable agreement between the calculated values and the experimental results, the differences could be reduced taking into account bowing effects in the calculation of allowing.

4. Conclusion

GaAsN thin film alloys deposited at low temperatures (450 °C) grow in a 3D mode. This growth mode results in films with a high density of crystal defects, a high built-in electric field, and strongly degraded optical characteristics. A 2D growth mode is obtained at high growth temperatures resulting in high quality pseudomorphic GaAsN layers.

Acknowledgments

This work was partially supported by CONACyT-Mexico and UC-MEXUS. The authors would like to thank the technical assistance of E. Gomez, Z. Rivera, and A. Guillen. A.P.M thanks the support by the program CUAUTHEMOC III SRE – Mexico.

References

[1] C. W. Tu, J, Phys. Condens. Matter. **13**, 7169 (2001).
[2] M. Reason, H. A. McKay, W. Ye, S. Hanson, and R. S. Goldman and V. Rotberg, Appl. Phys. Lett. **85**, 1692 (2004).
[3] D.E. Aspnes, Phys Rev. B **10**, 4228 (1974).
[4] F. H. Pollak. Surf. Interfase Anal. **31**, 398 (2001).

[5] J. Luyo-Alvarado, M. Melendez-Lira, M. Lopez-Lopez, and S. Goto, J. Vac. Sci. Technol. B **19**, 495 (2001).
[6] I. Vurgaftman and J. R. Meyer, J. Appl. Phys. 94, 3675 (2003).
[7] J. Misiewicz R. Kudrawiec, K. Ryczko, G. Sek, A. forchel, J. C.Harmand, and M. Hammar, J Phys.; Condens. Matter **16**, S3071 (2004).
[8] S. Adachi, H. Mori, and S. Ozaki, Phys. Rev. B **66**, 153201 (2002).
[9] G. Leibiger, V. Gottschalch, B. Rheinländer, J. S. Ik and M. Schubert, Appl. Phys. Lett. **69**, 1650 (2000).
[10] M. Munoz, Y. S. Huang, F. H. Pollak, H. Yang, J. Appl. Phys. **93**, 2549 (2003).